

## Research Paper

## Experimental Study of Identifying Emission Sources of Acoustic Signals on the Cylinder Body of a Two-Stroke Marine Diesel Engine

Xuan Thin DONG\*, Manh Hung NGUYEN

*Vietnam Maritime University*

Hai Phong, Vietnam; e-mail: nguyenmanhhung.vmu@gmail.com

\*Corresponding Author e-mail: dongxuanthin@gmail.com

(received May 21, 2020; accepted September 7, 2020)

In this paper, an experimental method was utilized to investigate acoustic emission (AE) characteristics and to identify emission sources of the nonlinear AE signal on the cylinder body of a large low-speed two-stroke marine diesel engine in real-working conditions on the sea in misfiring and normal firing modes. Measurements focused on the AE signal acquired in a transverse direction in low-frequency (20–80 kHz), medium-frequency (100–400 kHz) and high-frequency (400–900 kHz) ranges. The collected signals were analyzed on the crank angle and crank angle-frequency domains. The results showed that all potential sources of the nonlinear AE signal could be mapped in the low-frequency range. However, only the AE signal caused by the combustion process at around the top dead center could be well-observed in the medium-to-high-frequency range. The findings also revealed that in normal firing conditions, the AE energy radiated by friction in the down-stroke period was smaller than in the up-stroke process due to gas-sealing forces. Moreover, the AE energy in the misfiring condition was higher than in the normal firing state. These outcomes considerably contributed understandings to characteristics of friction and wear around the mid-stroke area of the cylinder on a two-stroke marine diesel engine.

**Keywords:** acoustic emission; two-stroke marine diesel engine; experimental method; low and medium-to-high frequency ranges; vibration.

## 1. Introduction

Currently, diesel engines have been widely used as the main power source of machinery in a variety of industrial fields such as marine offshore platforms, ships, transportation, mining, construction sites, etc. They have been also employed to generate the drive power for emergency generators in plants, hospitals, centres, and buildings. Therefore, the reliability of a diesel engine is the most important matter which has been concerned by many researchers. The unforeseen incident of engine's components could lead to efficiency reduction, partial damages or engine breakdowns. Especially, failures of the marine diesel engine of the propulsion shafting system could result in a terrible accident on the sea in bad weather conditions. In a diesel engine, cylinder and its processes are the most important issues which have been thoroughly considered for a long time. Piston-cylinder system and its complicated processes are the major sources of mechanical vibration, airborne acoustic and acoustic emission (AE). Accordingly, the component's situation

and characteristics of these processes could be determined based on monitoring mechanical vibration, airborne acoustic and AE signal. These signals are cyclostationarity and contain information about the engine state.

The mechanical vibration was successfully utilized for the detection and differentiation of the faults generated by a vibration signal acquired from the accelerometer (YUNUSA-KALTUNGO *et al.*, 2014; AHMAD, ALIREZA, 2019; JAFARIAN *et al.*, 2018). However, this method is sometimes hard to implement because it requires many accelerometers and different measurement positions to obtain the general engine condition. On the other hand, the vibration signals are easily contaminated by noise and need an effective signal processing method to get useful information (ELAMIN *et al.*, 2010; LIANG *et al.*, 1996). The airborne acoustic signal contains more information about the engine state; however, it is contaminated by noise as well. Thus, it is more challenging to derive a useful engine state information (BEN-SASI, 2005; ALBARBAR *et al.*, 2010). ALBARBAR *et al.* (2010) used three mi-

crophones around fuel injectors ( $120^\circ$  apart from each other) with a 25 cm optimized distance from the injector head to analyse fuel injection process characteristics. Nevertheless, it is hard to detect other acoustic sources such as exhaust valve and intake valve activities (ALBARBAR *et al.*, 2010).

Recently, acoustic emission (AE) has been used as a non-intrusive technique to monitor the mechanical events, components, and processes in a diesel engine. AE signals around the cylinder are radiated from multiple sources such as friction and wear induced by the sliding between piston rings and cylinder liners, cylinder pressure, air flows through the orifice, combustion, gas-sealing force applied on piston rings, blow-by and the valve activities. The AE signal is emitted under the elastic waves in a wide frequency range from very low frequencies up to 1 MHz. Owing to the complication of the AE signals generated by those sources, comprehensive analyses in many aspects should be taken into account. Injector's conditions in the injection process and the turbulent flow passing through the orifice to spray into the combustion chamber were surveyed in (AHMAD, ALIREZA, 2019; ALBARBAR *et al.*, 2010; DYKAS, HARRIS, 2017; LIN *et al.*, 2011; GILL *et al.*, 2000). The AE signal emitted by friction between the rings and cylinder liner was reflected in (WEI *et al.*, 2015; DOUGLAS *et al.*, 2006; DOUGLAS, 2007; BONESS, MCBRIDE, 1991; JIAA, DORNFELD, 1990; MECHEFSKE, SUN, 2001; PRICE *et al.*, 2005; SHUSTER *et al.*, 2000) by considering the piston position, moving direction, piston speed, etc. The movement of the exhaust and intake valves, as well as their working conditions such as leakage and valve operation fault, were also determined based on the AE signal (ELAMIN *et al.*, 2010; JAFARI *et al.*, 2014). To prove the relevance between AE signal and cylinder pressure, EL-GHAMRY *et al.* (2004) extracted and recovered the cylinder pressure from the AE signal. Combustion procedure was also studied using the AE signal at outer cylinders (WU *et al.*, 2015) or various points (DYKAS, HARRIS, 2017).

There were many types of diesel engines employed in experiments such as high-speed four-stroke one-cylinder, four-cylinders, low-speed two-stroke, car's engine, etc. (DYKAS, HARRIS, 2017). Mapping the location of AE signal's sources on the engine structure and in the crank angle domain was also a topic that attracted many researchers' concerns. For high-speed four-stroke diesel engines, NIVESRANGSAN *et al.* (2005a, 2005b) carried out two different studies related to the AE signal sources' identification. The former focused on finding out the location of AE emission sources based on the AE signal collected by nine sensors (NIVESRANGSAN *et al.*, 2005a). Meanwhile, the latter identified exhaust valves, inlet valves, and injectors events by analysing the AE signal obtained from an array of AE sensors (NIVESRANGSAN *et al.*, 2005b).

Also, ELAMIN *et al.* (2010) showed AE bursts generated throughout exhaust valve movements in the crank angle domain based on the crankshaft position and AE signal. Concerning the top dead centre (TDC) sensor and analysed signals acquired from four AE sensors, exhaust valves closing (EVC), inlet valve closing (IVC) and combustion events of each cylinder were also determined in the crank angle domain (WU *et al.*, 2015). The complicated process around TDC with fuel injection and combustion was presented by GILL *et al.* (2000) using high amplitudes; however, the results were not clear. The process around TDC separately pointed out for the fuel injection and combustion indicated that the combustion occurs after the injection period and has a higher amplitude (WEI *et al.*, 2015). In that research, AE signals emitted from the inlet valve opening (IVO), IVC, exhaust valve opening (EVO), EVC, friction, and wear were exhibited. Nevertheless, AE signals of EVO and friction were not clarified. Friction and wear sources were observed under motored mode by DOUGLAS *et al.* (2006).

In the case of a low-speed two-stroke diesel engine, the inlet valves are replaced by scavenging ports and there is an oil groove. Hence, the AE signal on the two-stroke diesel engine could be originated by friction and wear, the activities of EVO, EVC, injector opening (IO), injector closing (IC), fuel combustion (COMB), ring pack that passes oil grooves (OG) and scavenging ports (SP). The AE signal radiated from these sources was partially presented in several studies. The results in one cycle were analysed by DOUGLAS *et al.* (2006), but the afore-mentioned events were not mapped. According to the analysis results, the AE signal generated by the SP event can be guessed at the beginning and the end of the scavenging phase. The bursts around  $60^\circ$  after the TDC might be caused by the OG event; however, this event only appeared in the up-stroke process. In the up-stroke process, the phenomenon was not repeated. Additionally, the events around TDC (IO, IC, COMB) were not displayed. The high amplitude signals occurred during  $60^\circ$  around the TDC. Especially, the AE signal caused by friction and wear was not mentioned. More useful information on those sources was presented by BROWN *et al.* (2004). The AE signals caused by IO, IC, SP, OG events were determined specifically in this study. However, the SP and OG events were only detected in the down-stroke period. The AE signals generated by the sliding between the piston rings and cylinder liners, fuel combustion, and exhaust valve activities were not shown in detail. A drawback of this study is investigating those events in the time domain. Therefore, it is complex to exactly determine the time of each AE signal source in the crank angle domain. However, both studies emphasize that the AE signal propagating between individual cylinders was very small because of the large size of the diesel engine.

The literature review showed the lack of research focused on mapping all these sources of AE signal on the large low-speed two-stroke marine diesel engine. Besides, most of the studies were carried out under the experimental condition. Especially, the radiation of AE energy due to contact between ring packs and cylinder liners on the large two-stroke diesel engine has not been specifically addressed. In this paper, the AE signal on cylinder body of a large low-speed two-stroke six-cylinder marine diesel engine was measured in real-working conditions on the sea. The measurement was carried out in two frequency ranges, including low-range (20–80 kHz) and medium-to-high-range (100–900 kHz). The findings revealed that all sources of the AE signal could be detected in the low-frequency range. Meanwhile, only the events around TDC were displayed in the medium-to-high-frequency range. The frequency range of AE signals was also specified based on the crank angle-frequency domain. The results revealed that all sources could be discovered through

a suitable measuring position and frequency range. The combustion process (IO, COMB, IC) generated the AE signal with a higher frequency range than the remaining sources. It can be said that this study could make up for the shortcomings in the previous studies about investigating the AE signal generated around the mid-stroke on the large two-stroke diesel engine.

## 2. Experimental setup

A large low-speed two-stroke six-cylinder marine diesel engine (MAN B&W 6G60ME-C9.5) designed with 13500 kW at 96.2 rpm was used for measurement in this paper. The engine was attached to a propeller by intermediate and propeller shafts. Specifications of the engine, intermediate shaft, propeller shaft, and propeller are shown in Table 1.

Figure 1 shows the schematic diagram of the measuring system with the propulsion shafting system and data acquisition setup. The medium-to-high-frequency

Table 1. Specification of the propulsion shafting system.

|                     |                     |                            |
|---------------------|---------------------|----------------------------|
| Main engine         | Type                | MAN B&W 6G60ME-C9.5        |
|                     | Power               | 13,500 kW                  |
|                     | MCR                 | 96.2 r · min <sup>-1</sup> |
|                     | Firing order        | 1 5 3 4 2 6                |
|                     | Exhaust valve open  | 110–120 degrees after TDC  |
|                     | Exhaust valve close | 110–150 degrees before TDC |
| Turning wheel       | Moment of inertia   | 15,000 kg · m <sup>2</sup> |
|                     | Weight              | 5,467 kg                   |
| Propulsion shafting | Intermediate shaft  | ϕ 475 mm × 10,375 mm       |
|                     | Propeller shaft     | ϕ 605 mm × 7,568 mm        |
| Propeller           | Type                | Fixed Pitch Propeller      |
|                     | Weight              | 26,000 kg                  |
|                     | No. of blades       | 4                          |
|                     | Diameter            | 7.2 m                      |

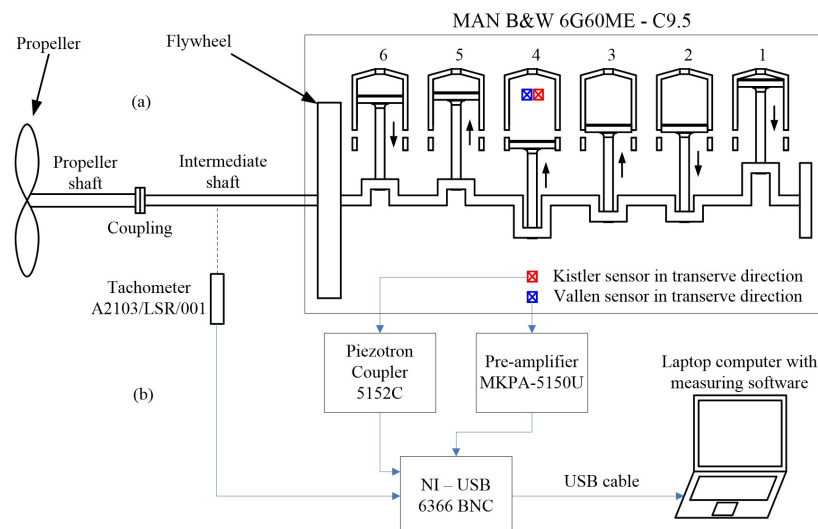


Fig. 1. Diagram of the measuring system; (a) propulsion shafting system, (b) data acquisition set up.

vibration in the transverse direction of cylinder four was examined by an Acoustic Emission sensor attached to the cylinder body by a hold-down magnetic as shown in Fig. 2. The AE Vallen sensor type VS 30-V was combined with preamplifier MKPA-5150U to measure the vibration in a range from 20 kHz to 80 kHz and Kistler sensor type (Model 8152C1050500) associated with Piezotron Coupler 5152C to detect the vibration in a range between 100 kHz and 900 kHz. A laser tachometer A2103/LSR/001 with one-pulse-per-revolution was utilized to measure shaft speed as well as to cut vibration signals. Because of the low shaft speed, any influence of fluctuation in engine speed can be exclusive. The AE signals were sampled at 2 MS/s by using NI – USB 6366 BNC device.

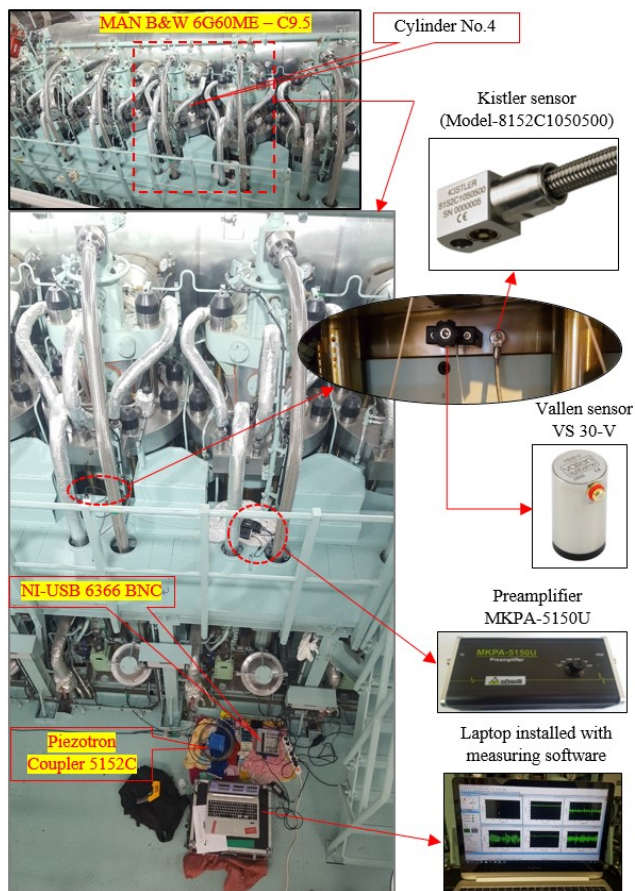


Fig. 2. Installation layout of experimental equipment in the real-working condition on the sea.

Two AE sensors were attached to the external liner of cylinder No. 4 (in the middle of a distance from the mid-stroke to the combustion chamber) in the transverse direction. According to the results of BROWN *et al.* (2004), this position could be suitable to detect all AE sources inside the cylinder. To prevent damages to the sensors from high temperatures of the cylinder body (approximately 110°C), these sensors were only mounted on the cylinder body for a short

time (less than five minutes). Moreover, Preamplifier MKPA-5150U and Piezotron Coupler 5152C not only supplied power to the sensors but also converted the AE to voltage signals. After that, the NI-6366 device received data under the analog voltage and converted them to digital data. The data were sent to a computer through a Universal Serial Bus (USB) cable. A laptop computer installed with a monitoring software was employed for this measurement. To avoid the impact of unwanted noises, all equipment was positioned near the main engine (see Fig. 2) to ensure that the connecting cables were as short as possible.

The tachometer signal was sent to channel 0 of the NI-6366 device to measure the shaft speed. Meanwhile, the raw AE signals collected by the Kistler and Vallen sensors were transferred to the NI device on channel 1 and 2, respectively. For the monitoring software, the sampling rates were set to 2 MS/s for all channels. Calculating the shaft speed, displaying the real-signal on the monitoring interface and recording the data were simultaneously done by the computer. Also, the measured data were recovered and cut within one revolution of the crankshaft for further analyses.

This measurement was carried out during the official sea trial of a new vessel at a calm sea organized by Hyundai SAMHO shipyard, Mokpo city, South Korea. According to the sea trial procedure, the vibration measurement was carried out from minimum to maximum continuous rating (MCR) of the diesel engine at each 2 rpm in the normal firing. In the case of misfiring mode, due to safety reasons, the maximum speed measured is smaller than in the normal firing state. Thus, to investigate and compare the vibration between two modes, this experiment was conducted at the same speed in both operating modes, including 40, 50, 60, and 70 rpm.

### 3. Analysis methodology

Based on the tachometer signal, raw data were collected in one revolution to detect differences between the vibration signals. The comprehensive comparison between the two operation modes was carried out in three ways. Firstly, real signals of both operation modes were compared in the crank angle domain. Secondly, two condition indicators, RMS and kurtosis, were applied for every one-degree of crankshaft angle in one revolution and for all samples in one revolution. Finally, to investigate the characteristics of AE signals in the frequency domain, the vibration was analysed in the crank angle-frequency domain by applying Fast Fourier Transform (FFT) for every 6 degrees of crankshaft angle. Due to the very wide range of investigated frequency, the octave band frequency method and peak value were employed to clarify the results.

### 3.1. Root Mean Square (RMS)

RMS describes the energy content of the vibration signal. It is not sensitive to incipient incident components and is utilized to evaluate the overall condition of the material (ZHU *et al.*, 2014; VEČERŮ *et al.*, 2005). With digital signals, the RMS is presented by:

$$x_{\text{RMS}} = \sqrt{\frac{1}{n} (x_1^2 + x_2^2 + \dots + x_n^2)}, \quad (1)$$

where  $x_{\text{RMS}}$  is the root mean square value of the analog signal,  $x = \{x_1, x_2, \dots, x_n\}$  is the set of  $n$  values  $x_i$ .

### 3.2. Peak amplitude

Peak value (or peak amplitude) is the concept widely used by researchers and analysts. It is the maximum instantaneous value measured from the zero level of alternative function or vibration signal during a specified time interval. The peak value is measured in both positive (+) and negative (–) signal.

### 3.3. Kurtosis

Kurtosis is a concept that was formally defined for the first time by PEARSON (1905). In this concept, kurtosis describes the shape of the amplitude distribution. The normal value of kurtosis equals 3. A kurtosis number greater than 3 indicates the sharp peaks. In contrast, the signal with flat peaks has a kurtosis number smaller than 3. Kurtosis formula is described by:

$$\text{Kurt}[X] = \frac{\frac{1}{n} \sum_{i=1}^n (x_i - \bar{x})^4}{\left(\frac{1}{n} \sum_{i=1}^n (x_i - \bar{x})^2\right)^2}, \quad (2)$$

where  $n$  is the number point of data set,  $x_i$  is the  $i$ -th point of data set,  $\bar{x}$  is the mean value of  $x$

$$\bar{x} = \frac{1}{n} \sum_{i=1}^n x_i. \quad (3)$$

### 3.4. Octave band

Octave band is a nonlinear algorithm used to divide the whole frequency range into sets of frequencies, called bands. Each band covers a specific range of frequencies. For this reason, the original band is considered as an octave when the upper band frequency is twice the lower band frequency. It is similar to a band-pass filter. The whole passband encompasses an octave. The upper band edge frequency equals twice the lower band edge one. The centre frequency  $f_c$ :

$$f_c = \sqrt{f_1 \cdot f_2}, \quad (4)$$

where  $f_1$  is the upper band edge frequency and  $f_2$  is the lower band edge frequency. According to octave

band definition,  $f_c$  is the centre frequency of an octave band and:

$$f_{\text{min}} = \frac{f_c}{\sqrt{2}}, \quad (5)$$

$$f_{\text{max}} = \sqrt{2}f_c, \quad (6)$$

where  $f_{\text{min}}$  is the lower frequency and  $f_{\text{max}}$  is the upper one.

In this study, to investigate characteristics of AE signals in the frequency domain, the AE signals were sequentially processed every six degrees and the FFT formula was applied to solve the collected signals. The frequency of the FFT result was ranged from 0 to 1 MHz. Because the desired frequency range was relatively broad, the octave band frequency (with an octave number 1/80) and peak value were used to analyse the result more accurately. The selected centre frequency was also an initial value of each frequency range. Table 2 presents an example of the octave band frequency in the medium-frequency range. For more specific measurements, the octave band algorithm divided the desired frequency range into 80 bands. Then, the peak value was employed on each band to reduce the resolution of the FFT result.

Table 2. Octave band frequency with an octave number 1/80 and a centre frequency of 100 kHz.

| Number of bands | Lower frequency [Hz] | Centre frequency [Hz] | Upper frequency [Hz] |
|-----------------|----------------------|-----------------------|----------------------|
| 1               | 99 567               | 100 000               | 100 434              |
| 2               | 100 434              | 100 870               | 101 308              |
| 3               | 101 308              | 101 747               | 102 189              |
| 4               | 102 189              | 102 633               | 103 078              |
| 5               | 103 078              | 103 526               | 103 975              |
| ...             | ...                  | ...                   | ...                  |
| 76              | 190 692              | 191 520               | 192 352              |
| 77              | 192 352              | 193 187               | 194 026              |
| 78              | 194 026              | 194 868               | 195 714              |
| 79              | 195 714              | 196 564               | 197 417              |
| 80              | 197 417              | 198 274               | 199 135              |

## 4. Results and discussion

### 4.1. Comparison of AE signals in the crank angle domain between the misfiring and normal firing modes

This study aims to investigate the vibration in the transverse direction at the cylinder body of a marine diesel engine. As mentioned in the previous part, the AE signal on the cylinder body could be generated from multiple sources. These sources were divided into

two groups, including mechanical activities and the remaining factors, to separately examine their influence. Firstly, the mechanical activities group will be investigated under the misfiring condition. Then, the remaining elements will be processed under the normal firing state.

In this study, the analysis results were collected through the official sea trial process. The engine was operated at a minimum continuous rating. When all parameters were set, the speed increased in value at every 2 rpm and was kept for a few minutes to gather the recording data. At first, the experiments were performed in the misfiring condition at various engine speeds, such as 40, 50, 60, and 70 rpm. The similar tests were carried out at the normal firing condition. For the tests in the misfiring state, the fuel sprayed into the cylinder No. 4 was cut while all other processes were unchanged. It means that the piston No. 4 was driven (or motored) by the crankshaft. The measured AE sig-

nals in the time domain were firstly converted into the data in the angular domain based on the tachometer signals. Because all the AE signals were monitored during an engine cycle and the two-stroke diesel engine completed its operating cycle in one crankshaft's revolution. Therefore, the measured signals were collected within one cycle. The vibration results in one revolution monitored by the Vallen sensor and Kistler sensor are shown in Figs 3 and 4, respectively. According to these figures, fluctuations of the AE events in association with the engine operation process can be easily observed.

In comparison between Figs 3a and 3b, it can be seen that in the low-frequency range, the vibration signal at around  $160^\circ$  was caused by the injection and combustion processes. Meanwhile, the vibration concentrated at around  $70^\circ$  and  $240^\circ$  might be generated

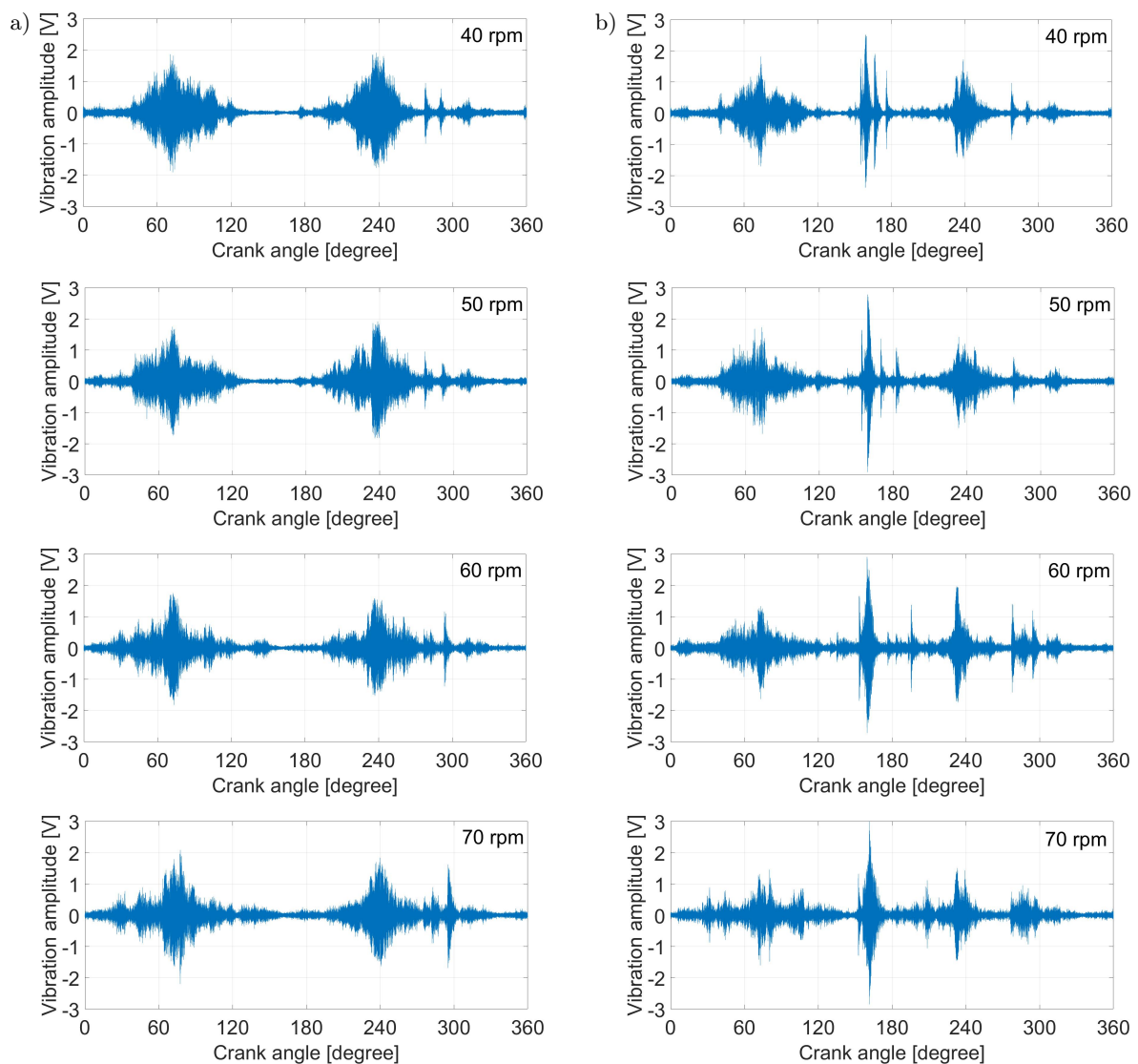


Fig. 3. The vibration results from 20 kHz to 80 kHz extracted on the cylinder body No. 4 in a transverse direction in the crank angle domain, including the misfiring mode (a) and the normal firing mode (b).

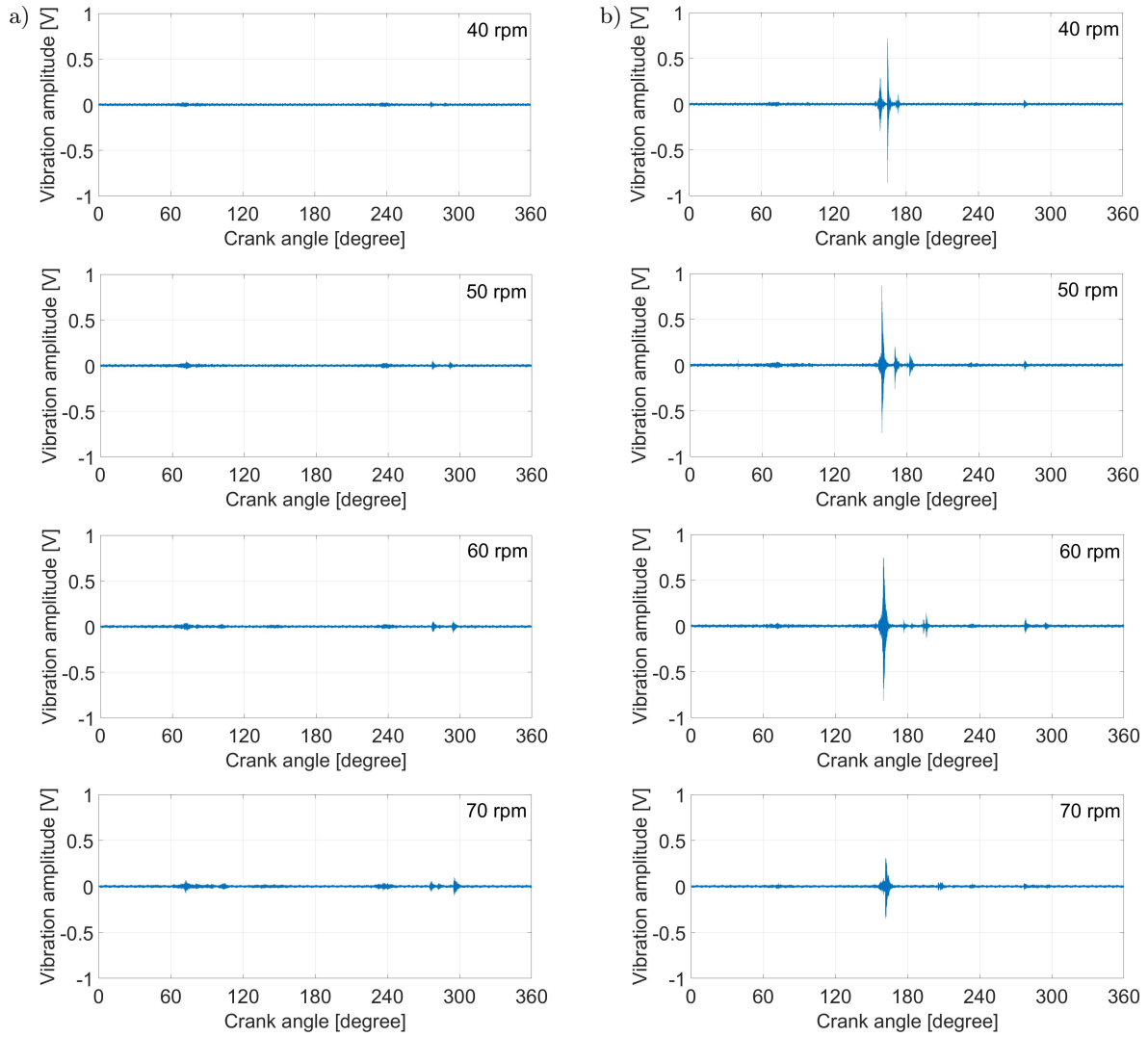


Fig. 4. The vibration results from 100 kHz to 900 kHz extracted on the cylinder body No. 4 in a transverse direction in the crank angle domain, including the misfiring mode (a) and the normal firing mode (b).

by the friction at the ring/liner interface around the mid-stroke and the remaining signals were emitted from the valve activities. For the misfiring condition, the amplitude of AE signals slowly decreased at crank angles from  $50^\circ$  to  $110^\circ$  and from  $200^\circ$  to  $255^\circ$  when the engine speed increased. However, the vibration at  $70^\circ$  and  $240^\circ$  was unchanged. It indicated that the AE signal value obtained in the up-stroke process is similar to those in the down-stroke process at each speed.

In the case of normal firing operating modes, the vibration at  $70^\circ$  was higher than at  $240^\circ$  at low speeds. On the other hand, the AE signal in the down-stroke process occurred at a smaller angle than in the up-stroke process. The vibration obtained at  $70^\circ$  in the normal firing state was lower than in the misfiring mode.

In a range of medium-to-high-frequency, only the vibration generated by the combustion process was displayed obviously (Fig. 4b) whereas the vibration

caused by the valve activities and radiated by friction between piston rings and cylinder liner was detected with very small amplitudes. Moreover, the vibration at  $70^\circ$  in the misfiring condition increased proportionally with the engine speed. These results proved that the emission sources of the AE signal should be measured in the low-frequency range.

#### 4.2. Comparison of AE signal energy using RMS and kurtosis parameters

To estimate the energy of the AE signal (or lost energy) between two operation modes, the RMS value of the AE signals applied to one engine cycle was presented by Eq. (1). The kurtosis parameter was also employed to outline the shape of the amplitude distribution, as defined in Eq. (2). The analysis results were shown in Fig. 5. The RMS value in the misfiring state was higher than in normal firing mode in both

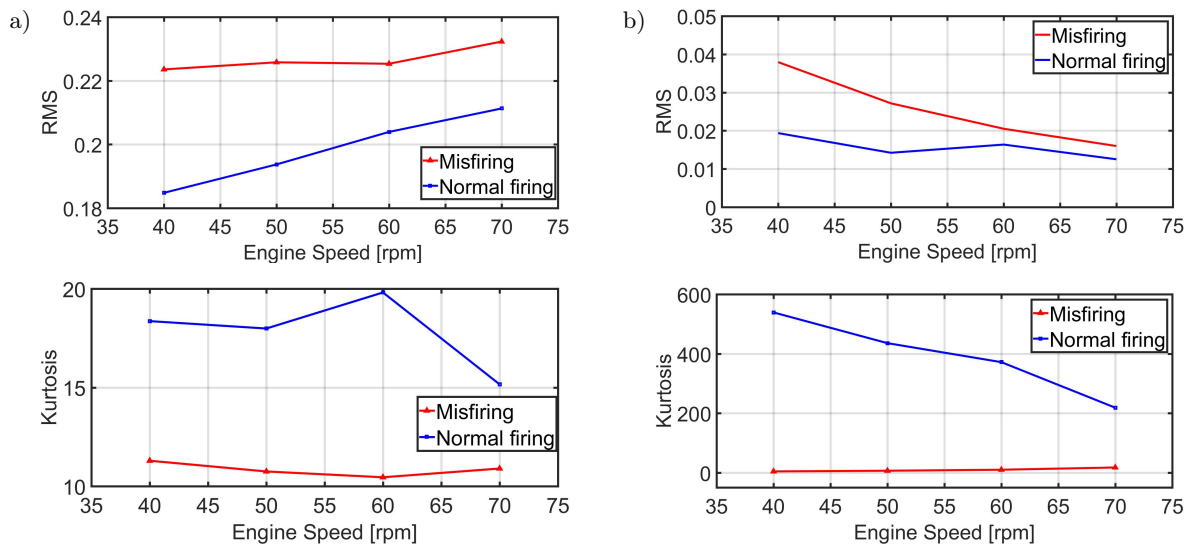


Fig. 5. The RMS and kurtosis values measured in the misfiring and normal firing conditions, for the low-frequency range (a) and medium-to-high-frequency range (b).

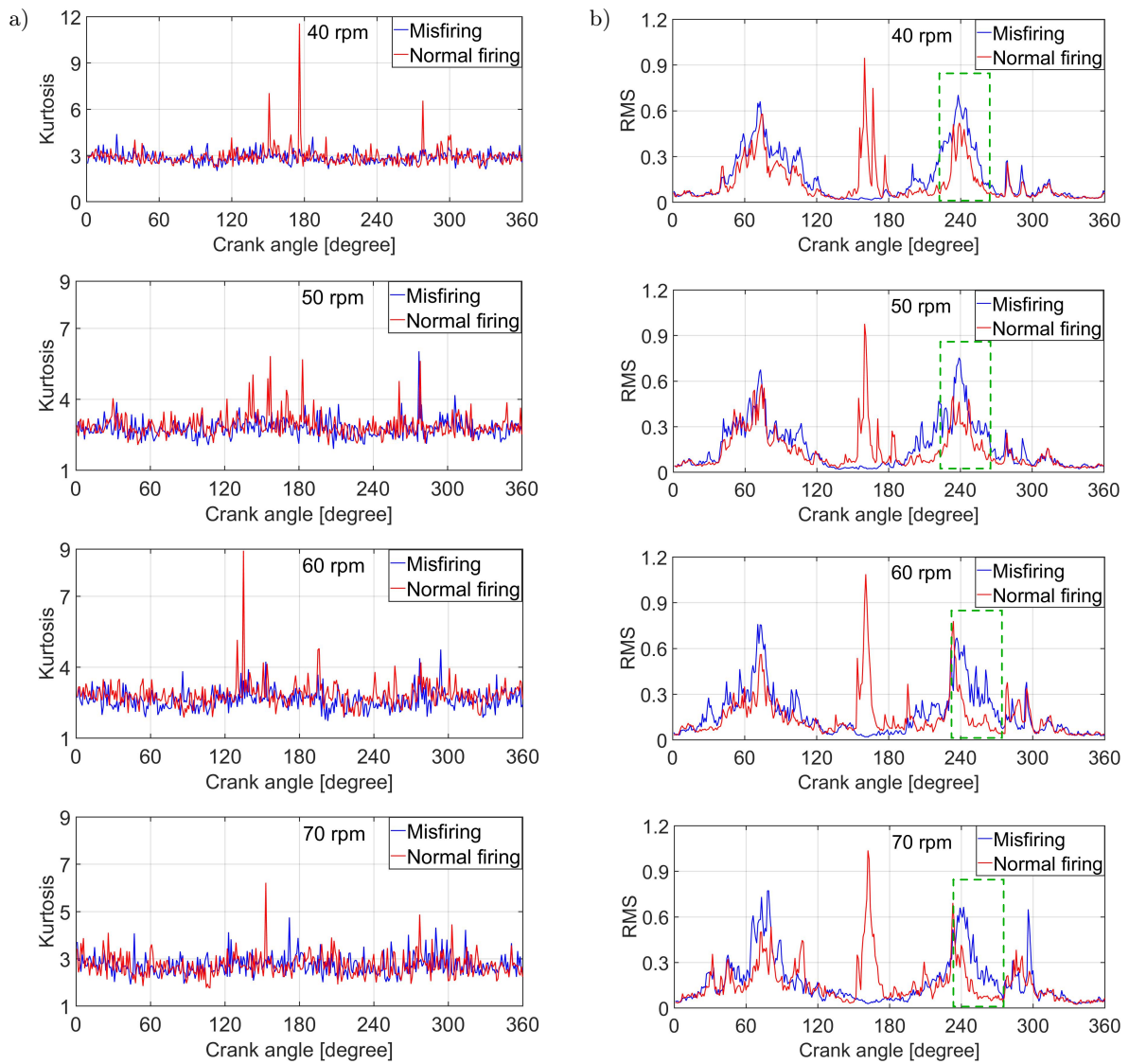


Fig. 6. RMS and kurtosis values used for the misfiring and normal firing conditions in a range of frequency from 20 to 80 kHz: a) kurtosis, b) RMS.

ranges of frequency. The higher value indicates that the energy loss in the motored case (due to friction) is more considerable than the running mode. The deviation between the two stages in both ranges of frequency gradually reduced when the engine's speed increased. When the speed rose, the AE energy decreased in the medium-to-high-frequency range for both operating modes; however, it went up in the low-frequency range. In contrast to the RMS value, the kurtosis value in the normal firing state was higher than in the misfiring state within all the frequency ranges. This point presented the signal sharpness in the crank angle domain and the existence of multiple shocks in the signal. To evaluate the characteristics of the AE signal more specifically, the RMS and kurtosis values were also employed on each crank angle, as shown in Figs 6 and 7.

It is shown that the kurtosis value in the normal firing mode was only higher than in the misfiring state at

a few degrees. At the remaining angles, the difference between the two operation modes was not obvious. It means that the sharpness and number of pulses at each degree of crank angle invariably altered in both states and mainly concentrated around the top dead centre (TDC) in the normal firing condition. The RMS results showed that the AE energy around the TDC in the normal firing mode was far higher than in the misfiring state. On the contrary, the RMS values from  $240^\circ$  to  $270^\circ$  (as marked by the small green dashed rectangles) in the misfiring mode were higher than in the normal firing mode whereas the difference in remaining crank angles was not apparent. These results revealed that the energy lost by friction in the running mode is smaller than in the motored mode.

Moreover, the medium-to-high-frequency range obtained the same kurtosis values as the low-frequency case. Conversely, only the RMS value around the TDC

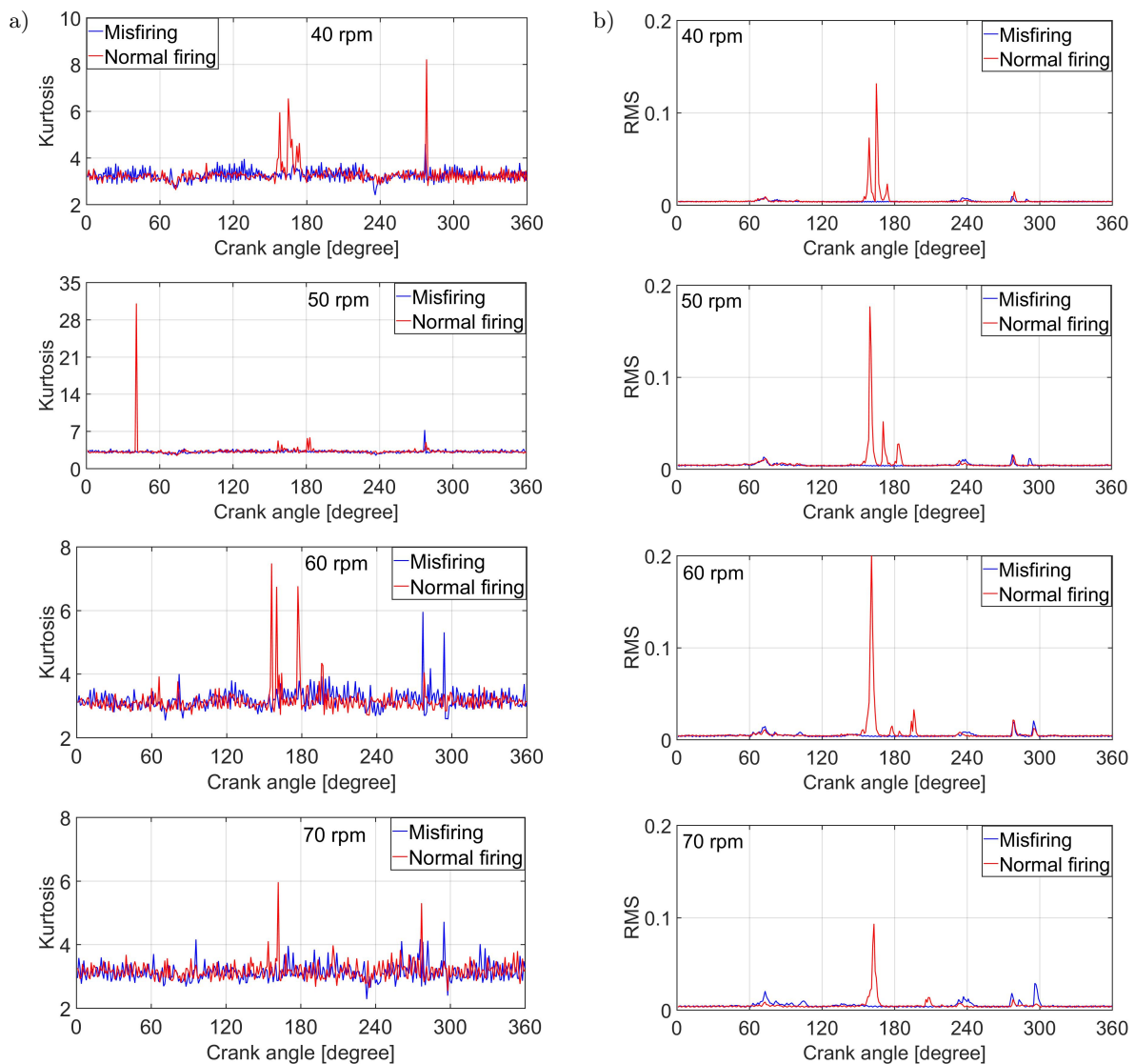


Fig. 7. RMS and kurtosis values used for the misfiring and normal firing conditions in a range of frequency from 100 to 900 kHz: a) kurtosis, b) RMS.

in the normal firing was higher than in the misfiring condition. Meanwhile, the difference between the two modes within the remaining angles was not clear. Additionally, the AE energy around the TDC at 70 rpm in the running mode declined by one half compared to the remaining speeds.

#### 4.3. Comparison of AE signals in the crank angle – frequency domain between the misfiring and normal firing modes

To investigate the vibration characteristics in the crank angle – frequency domain, the FFT algorithm was applied on every 6 degrees of data sets. The number of samples at every 6 degrees was not fixed at various speeds. The FFT method used for those samples created different findings in the dimension. Moreover, the output frequency of the FFT method was ranged from 0 to half of the sampling rate whereas the desired frequency range was fixed. Hence, the octave band al-

gorithm (as shown in Eqs (4)–(6)) and peak condition indicator were utilized to make the FFT analysis result much clearer. In both desired frequency ranges, the octave number of 1/80 was applied to the FFT results as shown in Figs 8 and 9. This solution was appropriate for a comprehensive comparison between the motored and running modes in all the frequency ranges. As seen from Fig. 8, the vibration around the TDC in the normal firing condition was higher than in the misfiring mode. Especially, the vibration at 60 kHz attained a higher amplitude. Meanwhile, the vibration at around 70° and 240° was identical in every condition. On the other hand, these signals in the normal firing were smaller than in the misfiring state. Additionally, the signal amplitude was gradually decreased in the frequency range of 20–60 kHz. However, these vibrations at speeds of 50 and 60 rpm were lower than at speeds of 40 and 70 rpm.

In the case of the medium-to-high-frequency range (see Fig. 9), the FFT results clearly showed the cha-

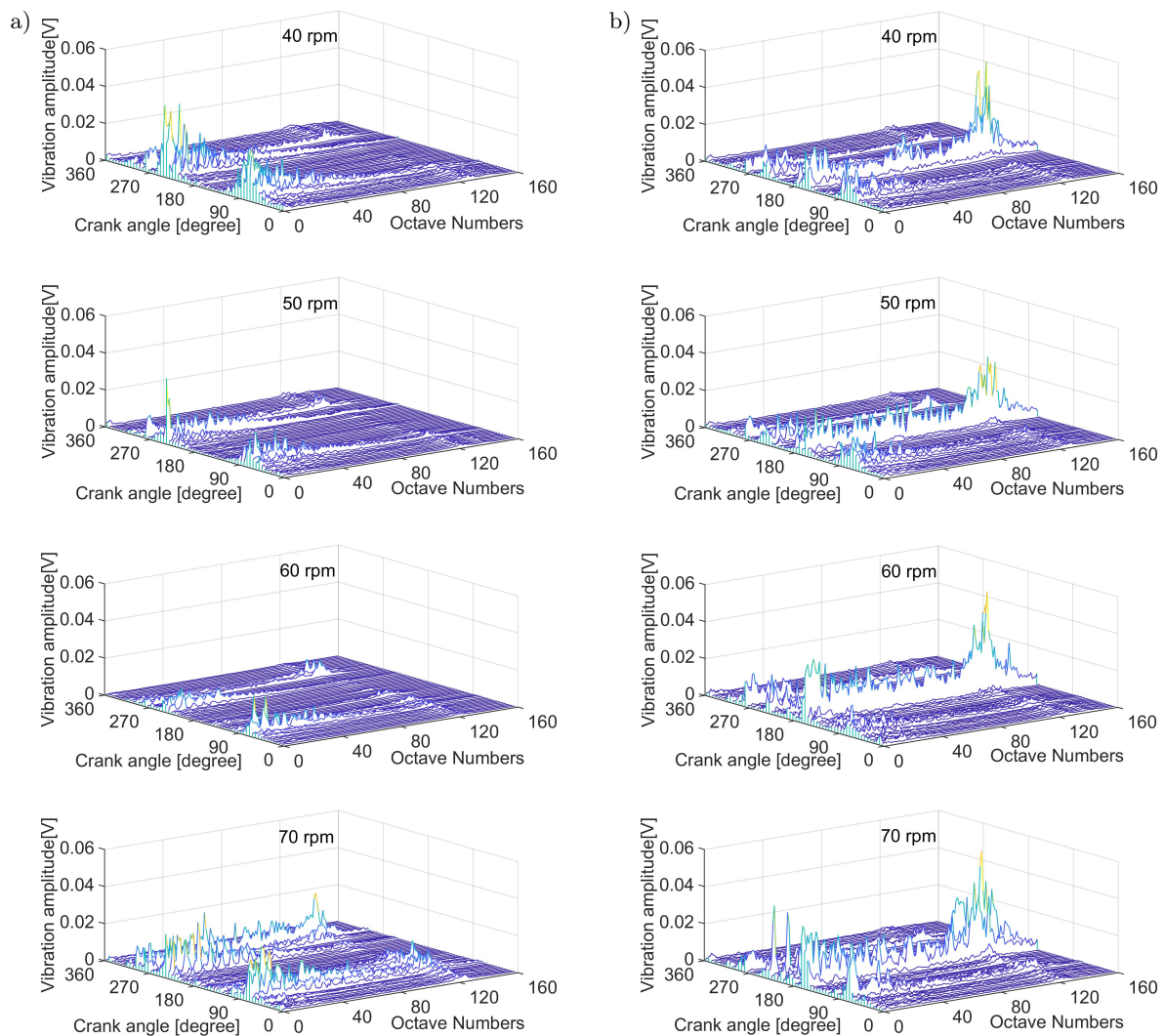


Fig. 8. FFT results with octave number 1/80 in the low-frequency range [1 = 20 kHz, 81 = 40 kHz, 160 = 80 kHz]: a) misfiring, b) normal firing.

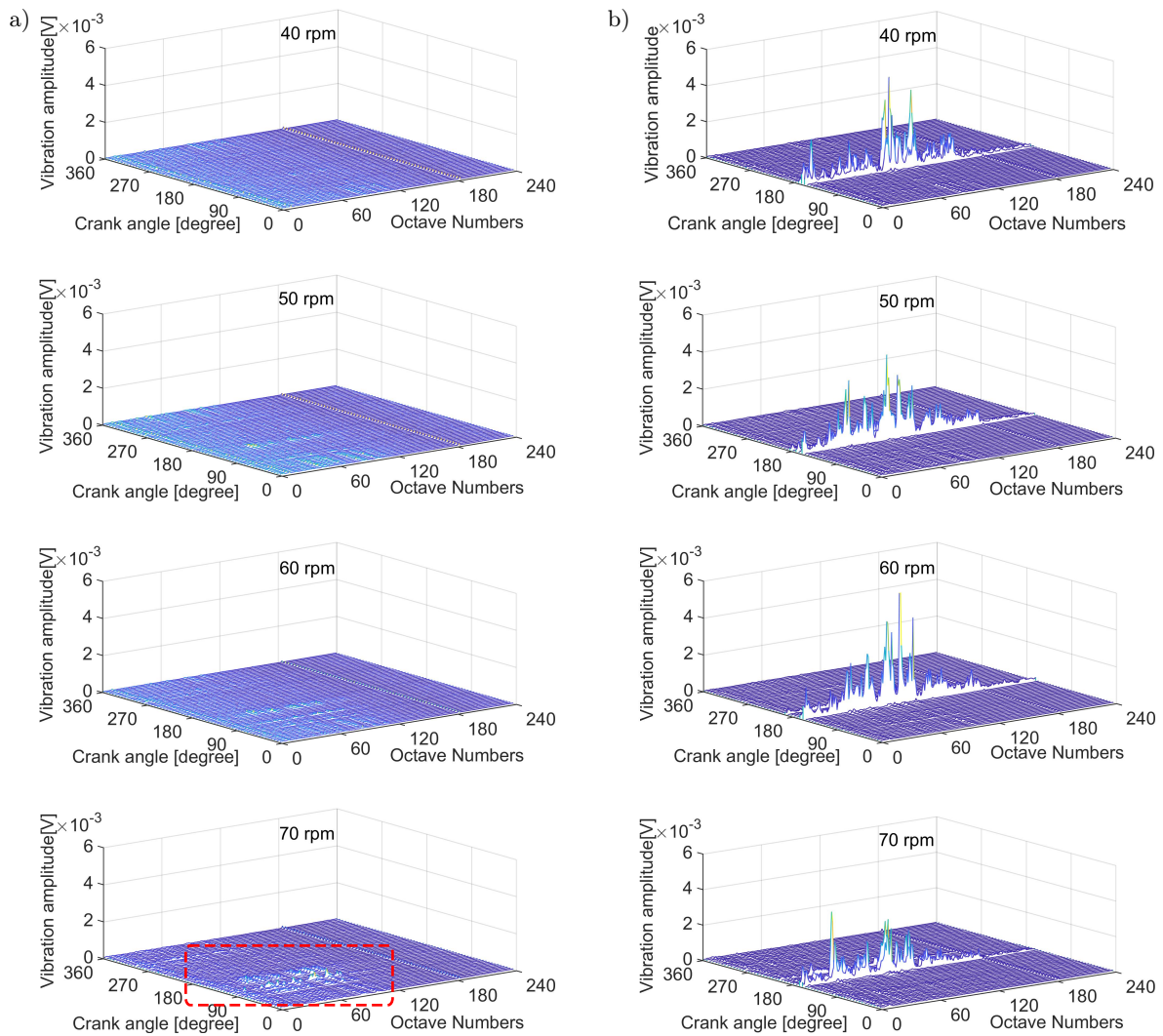


Fig. 9. FFT result with octave number 1/80 in the medium-high-frequency range [1 = 100 kHz, 81 = 200 kHz, 161 = 400 kHz, 240 = 800 kHz]: a) misfiring, b) normal firing.

characteristics of the combustion process whereas other sources of AE signal were not exhibited. The vibration of the combustion process was divided into three frequency bands of 200–350 kHz, 500–800 kHz and the remaining range. The highest-amplitude vibration concentrated on the first band. In the second band, the amplitude of vibration did not vary. In the remaining range, the amplitude of vibration increased gradually from 100 to 200 kHz but reduced slowly between 350 and 500 kHz. In the misfiring condition, there existed an area (marked by small dashed rectangles) which became more obvious at a higher speed. Nevertheless, this area did not exist in the normal firing operation mode. In case the attention focused only on the characteristics of the combustion process, experiments should be carried out on this frequency range. On the other hand, to investigate all sources of the AE signal, the low-frequency range could be considered as a proper selection.

#### 4.4. Discussion

In this paper, the measurement was carried with two frequency ranges (low and medium-to-high). It indicated that the AE signal generated by all sources, as mentioned in the early part, could be determined in the low-frequency range as shown in Fig. 10. The high-amplitude AE signal emitted by friction and wear appeared around the mid-stroke position in both operation modes. The AE signals radiated by other events such as ring pack passing the scavenging ports (SP), exhaust valve opening (EVO), exhaust valve closing (EVC), injector opening (IO), injector closing (IC), ring pack passing the oil groove (OG) and combustion were also presented. The signals caused by the SP events achieved small bursts because of a big distance from the sensor to the scavenging port. This is consistent with the conclusions of BROWN *et al.* (2004). Additionally, the burst caused by the SP event in the

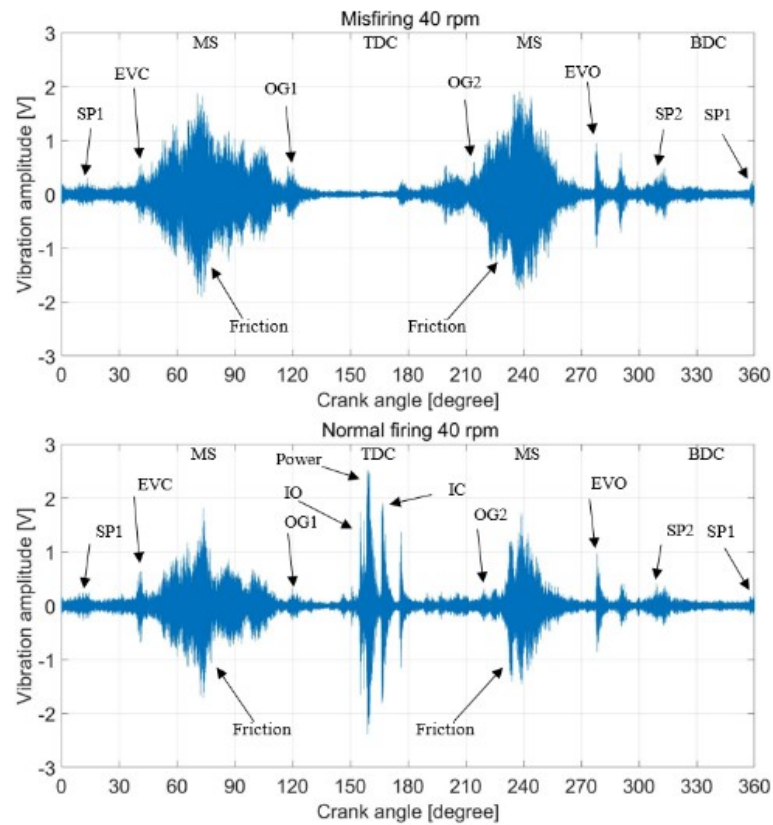


Fig. 10. The vibration signal extracted in the low-frequency range following the transverse direction of the cylinder No. 4 in the misfiring and normal firing operation modes; IO – injector opening; IC – injector closing; OG – ring pack passing oil groove; EVO – exhaust valve open; EVC – exhaust valve close; SP – ring pack passing scavenging ports; MS – around mid-stroke position.

down-stroke process was higher than in the up-stroke position. This could be explained by a noticeable difference between pressures inside and outside the cylinder. Especially, the vibration around the TDC only emerged in the normal firing condition. Furthermore, the amplitude of vibration at around the mid-stroke position in the normal firing mode was smaller than in the misfiring condition. It showed that the misfiring mode produced no power but also enlarged friction and wear. The reduction of vibration around the mid-stroke could be induced by the combustion gas. The high amplitude pulses that emerged around the mid-stroke are similar to the results presented in DOUGLAS *et al.* (2006) for the four-stroke diesel engine. The burst generated in the EVO event was higher than in the EVC event in both operating modes. Possibly, the AE signal was produced by another source when the exhaust valve started to open. Thus, the exact reason should be verified by another experiment in the future. Also, there remained several bursts in which the authors, in this paper, could not figure out their sources in  $175^\circ$  and  $290^\circ$ .

Figure 11 shows the AE signal in the medium-to-high-frequency range. It is seen that the high amplitude bursts mainly concentrated on the TDC position.

Only the AE signal caused by the EVO event could be detected with a small amplitude. Meanwhile, the existence of friction at the mid-stroke position was not obvious. This clarified the hypothesis about the existence of the AE signal generated by another source. The remaining sources did not appear in this case study. The combustion process radiated a vibration with the highest amplitude in both frequency ranges. The other sources such as the sliding of ring/liner, ring pack passing the scavenging ports and ring pack passing the oil groove did not consist of the medium-to-high-frequency vibration components. In both frequency ranges, the signal around the TDC was similar to the results presented in WEI *et al.* (2015). To investigate more specifically about the characteristic of the AE signal around the TDC, the injection process was separately investigated by a test without combustion. Other tests for the combustion process (incomplete or poor combustion) should be implemented as well. However, the procedure of the sea trial could not be changed because it must obey the regulations of safety and operation costs. This could be seen as a drawback of this study. However, in comparison with the existing studies, the analysis results of this study in the low-frequency range were clearer. Moreover, the

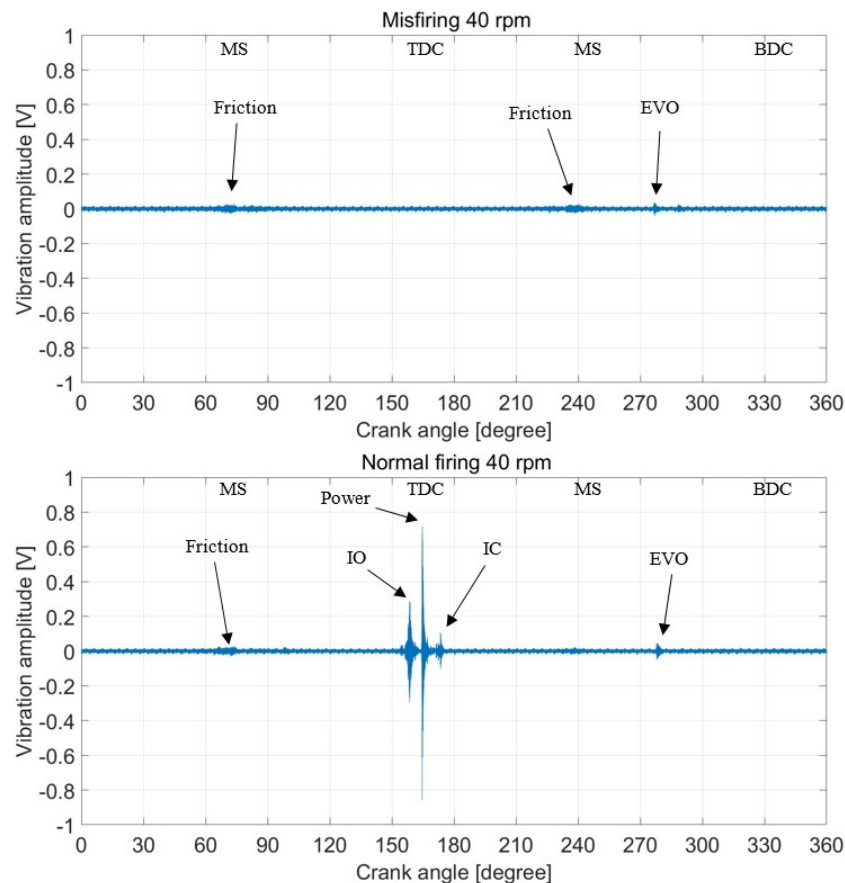


Fig. 11. The vibration signal extracted in the medium-to-high-frequency range following the transverse direction of the cylinder No. 4 in the misfiring and normal firing operation modes; IO – injector opening; IC – injector closing; EVO – exhaust valve open.

findings in the low-frequency range created a comprehensive view of all potential emission sources of the AE signal. According to the FFT result in the low-frequency range, the AE signal amplitude caused by friction was gradually decreased while increasing the frequency. Thus, the experiment should be carried out in low-frequency ranges when only focusing on friction and wear. In contrast, to investigate the characteristics of the injection and combustion processes, the measurement should be implemented in the medium-to-high-frequency range. This measurement could be used for other purposes such as investigating the characteristic of different types of lubrication oil, determining the time of each event within one engine cycle, and evaluating the quality of the injection process as well as the combustion state.

## 5. Conclusions

Acoustic emission signals at cylinder bodies on a two-stroke diesel engine were investigated in both operation modes in the frequency range up to 900 kHz. The results showed that all sources of the AE signal could be detected obviously in a suitable fre-

quency range of measurement. It consisted of friction and wears due to the interaction between ring pack and cylinder liner, injector opening/closing, combustion process, exhaust valve opening/closing, ring pack passing the scavenging ports and oil grooves.

All sources of the AE signal were identified clearly within the crank angle domain in the low-frequency range. In the medium-to-high-frequency range, only the processes happening around TDC were well-observed. Differences in the AE signals in both operating modes concentrated on the TDC area for both case studies. The kurtosis and RMS parameters at various speeds showed a difference between the two operation modes. In the low-frequency range, when the condition indicators were applied to each degree in one engine cycle, the RMS value was more useful to indicate the AE energy at each angle. In contrast, the kurtosis value was only advantageous around the TDC. According to these values, the AE energy radiated by friction in the misfiring mode was higher than in the normal firing when the piston moved from the TDC to the bottom dead centre(BDC).

The FFT method applied to each six-degree yielded the detailed outcomes in the crank angle-frequency do-

main. The results in the low-frequency range showed that the frequency of AE signal caused by friction and mechanical activities only reached 60 kHz whereas the injection and combustion processes could generate the frequency of AE signal from 20 kHz to 80 kHz. The findings in the medium-to-high-frequency range proved that the high-amplitude AE signal emitted from the injection and combustion processes could reach only 500 kHz and mainly focused on a range of 200–300 kHz. The signal in a frequency range higher than 500 kHz obtained a smaller amplitude.

Further research work will be conducted to investigate the AE signal in all directions at the cylinder body as well as at the injector area.

### Declaration of conflicting interests

The author(s) declared no potential conflicts of interest with respect to the research, authorship, and/or publication of this article.

### Acknowledgments

The author(s) acknowledge that this work was supported by Vietnam Maritime University. Also, we would like to thank the editor and the reviewers who gave constructive suggestions and careful reviews to us to improve the content of this paper.

### References

- AHMAD T.A., ALIREZA M. (2019), Fault detection of injectors in diesel engines using vibration time-frequency analysis, *Applied Acoustic*, **143**: 48–58, doi: 10.1016/j.apacoust.2018.09.002.
- ALBARBAR A., GU F., BALL A.D. (2010), Diesel engine fuel injection monitoring using acoustic measurements and independent component analysis, *Measurement*, **43**(10): 1376–1386, doi: 10.1016/j.measurement.2010.08.003.
- BEN-SASI A. (2005), *The exploitation of instantaneous angular speed for machinery condition monitoring*, Ph.D. Thesis, University of Manchester.
- BONESS R.J., MCBRIDE S.L. (1991), Adhesive and abrasive wear studies using acoustic emission techniques, *Wear*, **149**(1–2): 41–53, doi: 10.1016/0043-1648(91)90363-Y.
- BROWN E., DOUGLAS R., NIVESRANGSAN P., REUBEN R.L., ROBERTSON A., STEEL J.A. (2004), Source identification using acoustic emission on large bore cylinder liners, *Proceedings of the 26th European Conference on Acoustic Emission Testing*, pp. 637–643, Berlin, Germany.
- DOUGLAS R.M. (2007), *Monitoring of the piston ring-pack and cylinder liner interface in diesel engines through acoustic emission measurements*, Ph.D. Thesis, Heriot-Watt University.
- DOUGLAS R.M., STEEL J.A., REUBEN R.L. (2006), A study of the tribological behaviour of piston ring/cylinder liner interaction in diesel engines using acoustic emission, *Tribology International*, **39**(12): 1634–1642, doi: 10.1016/j.triboint.2006.01.005.
- DYKAS B., HARRIS J. (2017), Acoustic emission characteristics of a single cylinder diesel generator at various loads and with a failing injector, *Mechanical Systems and Signal Processing*, **93**: 397–414, doi: 10.1016/j.ymsp.2017.01.049.
- ELAMIN F., FAN Y., GU F., BALL A. (2010), Diesel engine valve clearance detection using acoustic emission, *Advances in Mechanical Engineering*, **2**: 1–7, doi: 10.1155/2010/495741.
- EL-GHAMRY M., STEEL J.A., REUBEN R.L., FOG T.L. (2004), Indirect measurement of cylinder pressure from diesel engine using acoustic emission, *Mechanical Systems and Signal Processing*, **19**(4): 751–765, doi: 10.1016/j.ymsp.2004.09.004.
- GILL J., REUBEN R.L., STEEL J.A., ASQUITH J. (2000), A study of small HSDI diesel engine fuel injection equipment faults using acoustic emission, *Journal of Acoustic Emission*, **18**: 1–6.
- JAFARI S.M., MEHDIGHOLI H., BEHZAD M. (2014), Valve fault diagnosis in internal combustion engines using acoustic emission and artificial neural network, *Shock and Vibration*, **2014**: Article ID 823514, doi: 10.1155/2014/823514.
- JAFARIAN K., MOBIN M., JAFARI-MARANDI R., RABIEI E. (2018), Misfire and valve clearance faults detection in the combustion engines based on a multi-sensor vibration signal monitoring, *Measurement*, **128**: 527–536, doi: 10.1016/j.measurement.2018.04.062.
- JIAA C.L., DORNFELD D.A. (1990), Experimental studies of sliding friction and wear via acoustic emission signal analysis, *Wear*, **139**(2): 403–424, doi: 10.1016/0043-1648(90)90059-J.
- LIANG B., GU F., BALL A. (1996), Detection and diagnosis of valve faults in recuperating compressors, *Proceedings of the 9th International Congress and Exhibition on Condition Monitoring and Diagnostics Engineering Management*, pp. 421–430, Sheffield, UK.
- LIN T.R., TAN A.C.C., MATHEW J. (2011), Condition monitoring and diagnosis of injector faults in a diesel engine using in-cylinder pressure and acoustic emission techniques, [in:] Su Z., Law S.S., Xia Y., Cheng L. [Eds], *Proceedings of the 14th Asia Pacific Vibration Conference – Dynamics for Sustainable Engineering – Vol. 1*, pp. 454–463, Department of Civil and Structural Engineering, The Hong Kong Polytechnic University, Hong Kong, <https://eprints.qut.edu.au/47625/>.

17. MECHEFSKE C.K., SUN G. (2001), Monitoring sliding wear using acoustic emission, *Proceedings of the 14th International Conference on Condition Monitoring and Diagnostic Engineering Management, COMADEM*, pp. 57–65, Manchester, UK.
18. NIVESRANGSAN P., STEEL J.A., REUBEN R.L. (2005a), Acoustic emission mapping of diesel engines for spatially located time series – Part II: Spatial reconstitution, *Mechanical Systems and Signal Processing*, **21**(2): 1084–1102, doi: 10.1016/j.ymsp.2005.08.024.
19. NIVESRANGSAN P., STEEL J.A., REUBEN R.L. (2005b), Source location of acoustic emission in diesel engines, *Mechanical Systems and Signal Processing*, **21**(2): 1103–1114., doi: 10.1016/j.ymsp.2005.12.010
20. PEARSON K.R. (1905), Skew variation, a rejoinder, *Biometrika*, **4**(1–2): 169–212.
21. PRICE E.D., LEES A.W., FRISWELL M.I. (2005), Detection of severe sliding and pitting fatigue wear regimes through the use of broadband acoustic emission, *Proceedings of the Institution of Mechanical Engineers, Part J: Journal of Engineering Tribology*, **219**(2): 85–98, doi: 10.1243/135065005X9817.
22. SHUSTER M., COMBS D., KARRIP K., BUREK D. (2000), Piston ring cylinder liner scuffing phenomenon studies using acoustic emission technique, *Proceedings of the CEC/SAE Spring Fuels & Lubricants Meeting and Exposition*, pp. 901–913, Paris, France.
23. VEČEŘ P., KREIDL M., ŠMÍD R. (2005), Condition indicators for gearbox condition monitoring systems, *Acta Polytech*, **45**(6): 35–43, doi: 10.14311/782.
24. WEI N. *et al.* (2015), Characterisation of acoustic emission for the frictional effect in engine using wavelets based multi-resolution analysis, *Proceedings of 21st International Conference on Automation and Computing (ICAC)*, pp. 1–6, Glasgow, UK, doi: 10.1109/ICoAC.2015.7313961.
25. WU W., LIN T.R., TAN A.C.C. (2015), Normalization and source separation of acoustic emission signals for condition monitoring and fault detection of multi-cylinder diesel engines, *Mechanical Systems and Signal Processing*, **64–65**: 479–497, doi: 10.1016/j.ymsp.2015.03.016.
26. YUNUSA-KALTUNGO A., SINHA J.K., ELBHBAH K. (2014), HOS analysis of measured vibration data on rotating machines with different simulated faults, [in:] Dalpiaz G. *et al.* [Eds], *Advances in Condition Monitoring of Machinery in Non-Stationary Operations. Lecture Notes in Mechanical Engineering*, Springer, Berlin, Heidelberg, doi: 10.1007/978-3-642-39348-8\_6.
27. ZHU J., NOSTRAND T., SPIEGEL C., MORTON B. (2014), Survey of condition indicators for condition monitoring systems, *Proceedings of Annual Conference of the Prognostics and Health Management Society*, pp. 635–647, Texas, USA.